A Modeling Study of the Pore Size Evolution in Lithium-Oxygen Battery Electrodes

Xianglin Li[*,z]

Department of Mechanical Engineering, University of Kansas, Lawrence, Kansas 66044, USA

This study develops a statistics model that investigates the microstructural evolution of porous electrodes and couples the micro structural changes with a computational fluid dynamics model to simulate the discharge performance of an 800-μm-thick electrode at 1 A/m^2. This study considers the fact that pores that are too small to hold reactants, smaller than a critical pore size, do not contribute to the discharge of the battery. It is found that when the pore size of the electrode increases, the discharge capacity of the electrode first increases due to the improved mass transfer and then decreases due to the decrease of the effective surface area. For instance, when the critical pore size is set as 10 nm, the discharge capacity gradually increases from 86.6 to 214.8 mAh/g_{carbon} when the mean pore size of the electrode increases from 10 to 50 nm, followed by a capacity decrease to 150.8 mAh/g_{carbon} when the mean pore size further increases to 100 nm. This study also finds that alternating the discharge current between 0 (open circuit condition) and the setting current rate can increase the discharge capacity of the lithium-oxygen battery because the oxygen concentration in the electrode increases during the open circuit condition.
 [DOI: 10.1149/2.0921508jes]

Manuscript submitted April 6, 2015; revised manuscript received April 29, 2015. Published June 3, 2015.

The increasing energy demands from portable electronic devices and the target of 300 miles driving range of electric vehicles have placed tremendous pressure on current electrical storage systems. Electric storage technologies with very high specific energy are required in order to meet the ever increasing energy demand without significantly increase the weight of the energy storage system. The lithium-oxygen battery is considered as a promising energy storage technology for portable and transportation applications considering its exceptionally high specific energy. Within four types of lithium-oxygen batteries,[1] the battery using organic electrolyte has attracted the most attention.[2] Although the active intermediates may react with non-aqueous electrolytes and produce lithium carbonate, lithium hydroxide, and lithium alkyl carbonate,[3–6] the main product is expected to be Li_2O_2 [2]. The overall reaction happens during charge and discharge of a lithium-oxygen battery using organic electrolyte is:

$$2Li + O_2 \leftrightarrow Li_2O_2 \quad (3.1\ V)\,. \qquad [1]$$

The theoretical energy density of the lithium-oxygen battery is calculated to be 11,680 Wh (kg lithium)$^{-1}$ or 2,790 Wh (kg lithium and oxygen)$^{-1}$.[7] The measured specific energy of lithium-oxygen batteries reported in literature, however, is less than 10% of the theoretical specific energy.[8,9] The power, capacity and efficiency of batteries are restricted by the cathode gas diffusion electrode (GDE), which is typically made from carbon material, considering the high energy density of lithium metal and fast reaction rate of lithium electrode.[6,10–14] In particular, the low solubility and diffusivity of oxygen in non-aqueous electrolytes limit the current density and the capacity of the battery.[9,15–19] Meanwhile, pores with different sizes in the electrode have different impacts on the mass transfer due to the limited ion conductivity and oxygen diffusivity of the electrolyte and the fact that solid products produced during discharge passivate the electrode and impede mass transfer. Experimental studies have been carried out to investigate effects of mass transfer characteristics such as the porosity of the electrode,[20–23] solubility of oxygen in organic electrolytes,[24] diffusivities of oxygen and lithium ion,[24] and stability of electrolytes.[4,25] Since both lithium ion and O_2 have to migrate to the reaction sites to continue the reaction, micro-pores that are too small cannot facilitate the mass transfer. Several studies have investigated the performance of lithium-oxygen batteries with various pore size distributions.[26,20,27]

Tran et al.[26] prepared carbon materials with mean pore size from 2.3 to 5.5 nm using commercially available high surface area activated carbon materials. The 200-μm thick GDE, with a weight of 10 mg, was made from 90 wt% of carbon and 10 wt% of Teflon material. This study hypothesized that micro-pores were blocked by the discharge product, Li_2O_2, so that the surface area of those pores were not available for the electrochemical reaction. The discharge capacity was found to increase almost linearly with the increase of average pore diameter from 2.3 to 5.5 nm. The maximum capacity of about 300 mAh/g was achieved at the average pore size of 5.5 nm when the discharge current was 1 mA/cm^2.

Younesi et al.[20] made 40-μm-thick electrodes from carbon super P carbon and Kynar2801 with different carbon contents from 0.2 to 0.8. It was found that the binder (Kynar) blocked the majority of pores smaller than 30 nm, decreased the surface area and pore volume and decreased the discharge capacity of the battery. The authors also concluded that the discharge capacity of the battery is mainly determined by meso-pores larger than 30 nm.

Ding et al.[27] investigated the discharge capacity of lithium-oxygen batteries using commercially available carbon materials. There is no clear correlation between the discharge capacity and the surface area or the porosity of the electrode, but the discharge capacity is found to increase with an increasing pore size. The authors also synthesized meso- and macro- porous carbons with pore size from 2.4 nm to 100 nm using phenol formaldehyde resin and silica spheres with different sizes. The measured discharge capacity of electrodes made from these home-made porous carbons first increased with the increasing pore size from 2.4 nm to 80 nm, followed by a decreased capacity when the pore size was further increased to 100 nm. A maximum discharge capacity of 7169 mAh/g was achieved at a pore size of 80 nm.

In the above experimental studies, the amount of electrolyte, type of electrolyte, morphology of the electrolyte, thickness of the electrode, current density etc. all affect the mass transfer in porous electrode and complicate studies of pore sizes. The critical size of the micro pores reported in literature is not consistent and the crucial mechanism that couple the mass transfer with electrochemical reactions in micro-, meso- and macro- pores in porous electrode is still unclear.[28] As a complement to experiments, modeling studies on the transport phenomena in lithium-oxygen batteries can screen out irrelevant factors and study the impact of individual parameters in detail.

J. Read et al.[24] pioneered the one-dimensional model of mass transfer in lithium-oxygen batteries and simulated the oxygen concentration along the depth of carbon electrode at steady state. The simplified model assumed that the porosity of the electrode did not change with Li_2O_2 production and the discharge reaction was linearly proportional

*Electrochemical Society Active Member.
zE-mail: xianglinli@ku.edu

to the oxygen concentration. Model results indicated that the oxygen concentration decreased along the depth of the electrode due to reactions and the concentration decreased faster at higher discharging current rates. The increase of both oxygen solubility and diffusivity through the electrode and electrolyte increases the oxygen concentration and decreases the discharge over-potential. The model developed by Sandhu et al. and Albertus et al.[29,30] considered the decrease of pore radius due to the accumulation of Li_2O_2 solid. The decrease rate of the pore size is proportional to the discharging current rate. Their model results also showed that the specific capacity decreased with both the increase of discharge current and the increase of electrode thickness. Andrei et al.[31] simulated oxygen and lithium ion concentrations and porosity distributions along the cathode carbon electrode and proposed several approaches to optimize the structure of the cathode electrode: increase the oxygen diffusivity and solubility; increase the catalyst activity; use catalysts with non-uniform activity along the electrode; and apply partially wetted cathode electrode. Sahapatsombut et al.[32] simulated the charge and discharge of a lithium-oxygen battery based on the concentrated binary electrolyte theory. The battery capacity was found to be affected by the solubility of oxygen, porosity and thickness of electrode and reaction rates. In analogy to the ice formation in proton exchange membrane fuel cells, Wang[17] proposed a reaction surface coverage model to account for Li_2O_2 precipitation during discharge and developed a one-dimensional model of lithium-oxygen batteries.

Xue et al.[33] considered the growth of Li_2O_2 film during discharge in their one-dimensional model. The model assumed that the thickness of the Li_2O_2 film followed a normal distribution between 5 and 10 nm. Once the thickness of the Li_2O_2 film exceeds 5 nm, the active surface area will be sharply decreased due to the increase of the resistance for electrons to tunnel through Li_2O_2 films. Xue et al.[34] recently included two mechanisms of oxygen reduction reactions: one mechanism produces a Li_2O_2 thin film on the electrode surface and the other generates Li_2O_2 particles in large open space (larger than 125 nm) of the electrode. An escape factor, which varies from 0 to 1, is introduced to quantitatively evaluate the possibility of Li_2O_2 escapes the electrode surface. Although the discharge performance is very sensitive to this escape factor, it's difficult to accurately estimate the value of the escape factor. Instead, values of escape factor are fitted with experimental data in their study and these values are found to decrease with increasing discharge current rates.

Meanwhile, a few model studies capture the two-dimensional mass transfer characteristics of a lithium-oxygen battery considering the non-uniform oxidant and production distributions in the in-plane direction of electrodes. Our previous studies consider the fact that mesh and end plates next to the cathode electrode inevitably block part of the oxygen path way and impede the mass transfer.[16,35] With other parameters remain the same, the capacity of the battery decreased by 75% when the open ratio decreased from 100% to 50%. Furthermore, the mass transfer could be significantly enhanced by forced convection of electrolyte driven by the pressure gradient between adjacent channels.[35] The model study also indicated that electrodes with a higher porosity on the air side yields a higher capacity, these finding was proved by the experimental study by Tan et al.[22] Wang and Cho[36] recently developed a multi-dimensional model considering the oxygen delivery in flow channels and found out that the electrode is not fully utilized during discharge, particularly under high discharging current rates.

Although some of the above mentioned model considered the Li_2O_2 precipitation and electrode passivation, none of the studies considered the dynamic change of pore size in the electrode. Furthermore, above models assumed that all pores in the electrode contribute to the discharge. The transport mechanism in micro-, meso- and macro-pores is still unclear and there is no accepted criterion to quantitatively determine impacts of different pores. This study will carry out multi-scale model simulations, which couple a novel micro-scale statistics model and a macro-scale computational fluid dynamics (CFD) model to investigate the evolution of pore size distribution in battery electrodes and its effect on the mass transfer and battery capacity.

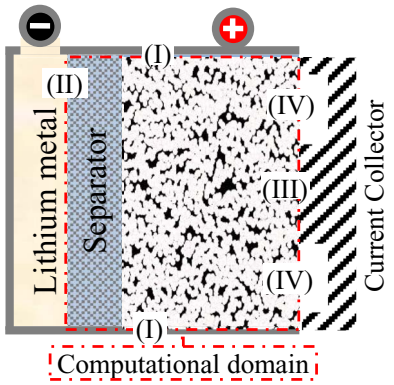

Figure 1. A lithium-air battery using organic electrolytes.

Model Development

We have developed a two-dimensional, transient, non-isothermal CFD model to simulate the heat and mass transfer characteristics in the electrolyte and cathode air electrode of a Li-air battery using organic electrolyte.[16,35] This study applies the CFD model to simulate the distribution of oxygen concentration, Li^+ concentration, reaction rate, and volume fraction of solid product. The novelty of this study is that properties of the porous electrode in the CFD model is determined by a statistics model that considers the change of the pore size distribution and critical pore size during discharge. The coupling between the CFD model and statistics model generates a unique multi-scale simulation tool to investigate the transport phenomena in porous electrodes.

Computational domain.— The computational domain of the model includes the separator and the cathode air electrode filled with the electrolyte, as shown within the dashed line in Figure 1. The ratio of the width of the channel to the overall width of the current collector (including both the channel and the rib) is defined as the open ratio of the current collector. If not otherwise specified, the open ratio of the current collector is set as 0.5 in this study to simulate practical applications.

Assumptions.—

1) The over-potential of the anode reaction is negligible;[11]
2) Electrolyte fully fills pores in the cathode electrode so that oxygen and lithium ion transfer in liquid phase (electrolyte) only;
3) Li_2O_2 deposits as a smooth film on the electrode surface.[37]
4) The flux of Li^+ at the lithium/electrolyte interface is proportional to the current density;
5) The thermal resistance of lithium metal and end plates made from metals are negligible due to their high thermal conductivity (21.9–84.8 W m^{-1} K^{-1}) compared with that of carbon (1.5 W m^{-1} K^{-1}).[38]

Governing equations.— The governing equations of heat and mass transfer, summarized in Table I, are similar to the governing equations in our previous studies.[16,35] The continuity equation in the porous media can be written as:

$$\frac{\partial(\varepsilon\rho_{EL})}{\partial t} + \nabla\cdot(\varepsilon\rho_{EL}\mathbf{u}) = \dot{m}_{Li+} + \dot{m}_{O_2} \quad [2]$$

where $\dot{m}_{Li+}$ and $\dot{m}_{O_2}$ are consumption rates of lithium ion and oxygen, respectively. The concentration of lithium ion and dissolved oxygen are solved by:

$$\frac{\partial(\varepsilon\rho_{EL}\omega_{Li+})}{\partial t} = \nabla\cdot\left(\rho_{EL}D^{eff}_{Li+}\nabla\omega_{Li+}\right) - \nabla\cdot\left(\frac{i_{EL}t_+}{F}M_{Li+}\right) + \dot{m}_{Li+} \quad [3]$$

and

$$\frac{\partial(\varepsilon\rho_{EL}\omega_{O_2})}{\partial t} = \nabla\cdot\left(\rho_{EL}D^{eff}_{O_2}\nabla\omega_{O_2}\right) + \dot{m}_{O_2} \quad [4]$$

Table I. Governing equations of the computational fluid dynamics model.

	Equation	Source term
Mass	$\frac{\partial(\varepsilon\rho_{EL})}{\partial t} + \nabla\cdot(\varepsilon\rho_{EL}\mathbf{u}) = \dot{m}_{Li+} + \dot{m}_{O_2}$	$\dot{m}_{EL} = \dot{m}_{Li+} + \dot{m}_{O_2}$
Li^+	$\frac{\partial(\varepsilon\rho_{EL}\omega_{Li+})}{\partial t} = \nabla\cdot(\rho_{EL}D^{eff}_{Li+}\nabla\omega_{Li+}) - \nabla\cdot(\frac{i_{EL}t_+}{F}M_{Li+}) + \dot{m}_{Li+}$	$\dot{m}_{Li+} = -\frac{R_{ORR}}{F}M_{Li+}$
O_2	$\frac{\partial(\varepsilon\rho_{EL}\omega_{O_2})}{\partial t} = \nabla\cdot(\rho_{EL}D^{eff}_{O_2}\nabla\omega_{O_2}) + \dot{m}_{O_2}$	$\dot{m}_{O_2} = -\frac{R_{ORR}}{2F}M_{O_2}$
Energy	$\frac{\partial([\rho C_p]^{eff}T)}{\partial t} = \nabla\cdot(k^{eff}_T\nabla T) + \dot{m}_T$	$\dot{m}_T = R_{ORR}(E_0 - V)$

Where Effective diffusivity: $D_i^{eff} = D_i\varepsilon^{1-0.77\ln\varepsilon}$;

Effective heat capacity per volume: $[\rho C_p]^{eff} = (1-\varepsilon)\rho_{ED}C_{p,ED} + \varepsilon_{Li_2O_2}\rho_{Li_2O_2}C_{p,Li_2O_2} + (\varepsilon - \varepsilon_{Li_2O_2})\rho_{EL}C_{p,EL}$;

Effective thermal conductivity: $k_T^{eff} = (1-\varepsilon)k_{ED} + \varepsilon_{Li_2O_2}k_{Li_2O_2} + (\varepsilon - \varepsilon_{Li_2O_2})k_{EL}$;

Reaction rate: $R_{ORR} = (\frac{\omega_{Li+}}{\omega^{ref}_{Li+}})^2\cdot(\frac{\omega_{O_2}}{\omega^{ref}_{O_2}})\cdot k_{ORR}\cdot\frac{A_{ED}}{V_{ED}}\cdot\exp(\frac{\alpha_{ORR}F}{RT}\eta_C)$;

$k_{ORR}(T) = k_{ORR}(293\text{ K})\cdot\exp[\frac{E_{ORR}}{R}(\frac{1}{293} - \frac{1}{T})]$, and

$$k_{ORR}(293\text{ K}) = \begin{cases} i_0\cdot\frac{A_{eff}}{V_{ED}}\cdot(1-0.9\cdot\frac{q}{7}) & \text{for } q \le 7\ C/m^2 \\ 1.5245\ i_0\cdot\frac{A_{eff}}{V_{ED}}\cdot 10^{-0.02616q} & \text{for } q > 7\ C/m^2 \end{cases}.$$

The effective diffusivity, D_i^{eff}, is determined by the diffusion coefficients, D_i, porosity, ε, and tortuosity, τ, of the porous media:

$$D_i^{eff} = D_i\varepsilon^{\tau} \quad [5]$$

where the tortuosity is a function of porosity:[39]

$$\tau(\varepsilon) = 1 - 0.77\ln\varepsilon \quad [6]$$

The porosity of the electrode made from smaller carbon particles is likely to be lower than the porosity of the electrode made from larger carbon particles. In this study, the following correlation between the mean pore size and porosity is derived from the experimental data, Figure 2, published by Olivares-Marin et al.:[23]

$$\varepsilon = 0.0899\ln(d_{mean}) + 0.3661. \quad [7]$$

The second term on the right hand side of Eq. 3 considers the migration of Li^+, where i_{EL} is the current density and t_+ is the transference number of Li^+. The consumption rate in the species equations of Li^+, and O_2 are:

$$\dot{m}_{Li+} = -\frac{R_{ORR}}{F}M_{Li+} \quad [8]$$

$$\dot{m}_{O_2} = -\frac{R_{ORR}}{2F}M_{O_2} \quad [9]$$

where R_{ORR} is the reaction rate of the oxygen reduction reaction (ORR), and M is the molecular weight. The energy balance equation is expressed as:

$$\frac{\partial\left([\rho C_p]^{eff}T\right)}{\partial t} = \nabla\cdot\left(k_T^{eff}\nabla T\right) + \dot{m}_T \quad [10]$$

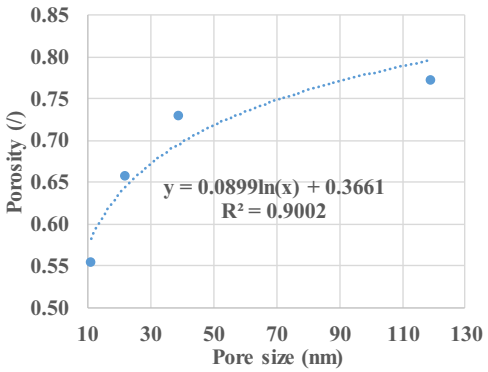

Figure 2. Experimental measurements of mean pore size vs. porosity.[23]

where the effective specific heat, $[\rho C_p]^{eff}$, and the effective thermal conductivity, k_T^{eff}, are related to the properties of the electrode, precipitated Li_2O_2, and electrolyte:

$$[\rho C_p]^{eff} = (1-\varepsilon)\rho_{ED}C_{p,ED} + \varepsilon_{Li_2O_2}\rho_{Li_2O_2}C_{p,Li_2O_2} + \left(\varepsilon - \varepsilon_{Li_2O_2}\right)\rho_{EL}C_{p,EL} \quad [11]$$

$$k_T^{eff} = (1-\varepsilon)k_{ED} + \varepsilon_{Li_2O_2}k_{Li_2O_2} + \left(\varepsilon - \varepsilon_{Li_2O_2}\right)k_{EL} \quad [12]$$

The local volume fraction of Li_2O_2, $\varepsilon_{Li_2O_2}$, is calculated based on the amount of accumulated Li_2O_2:

$$\varepsilon_{Li_2O_2}(t) = \frac{\int R_{ORR}\cdot dt}{2F}\frac{M_{Li_2O_2}}{\rho_{Li_2O_2}}. \quad [13]$$

The source terms used in the energy equations are related to the electrochemical reaction:

$$\dot{m}_T = R_{ORR}(E_0 - V) \quad [14]$$

where E_0 is the thermodynamic equilibrium voltage, 3.1 V, and V is the discharge voltage of the cell.

The local ORR rate of the Li-O_2 battery is determined by concentrations of lithium ion and oxygen, the standard constant rate of ORR, k_{ORR}, the surface area of the electrode, A_{ED}, per volume of electrode, V_{ED}, and the over-potential, η_c by the following equation:

$$R_{ORR} = \left(\frac{\omega_{Li+}}{\omega^{ref}_{Li+}}\right)^2\cdot\left(\frac{\omega_{O_2}}{\omega^{ref}_{O_2}}\right)\cdot k_{ORR}\cdot\frac{A_{ED}}{V_{ED}}\cdot\exp\left(\frac{\alpha_{ORR}F}{RT}\eta_C\right) \quad [15]$$

The effective surface area and the volume of the electrode are determined from the statistics model that will be described in section Microstructural evolution of the porous electrode. The standard rate constant, k_{ORR}, in the above reaction is a function of temperature:

$$k_{ORR}(T) = k_{ORR}(293\text{ K})\cdot\exp\left[\frac{E_{ORR}}{R}\left(\frac{1}{293} - \frac{1}{T}\right)\right] \quad [16]$$

where E_{ORR} is the activation energy of the ORR, which has the value of 21 kJ mol^{-1} as an approximation.[40] In all the calculations of current work, initial temperature is set at 293 K. The effect of the electrode passivation caused by the Li_2O_2 precipitation during discharge is considered by a segmental equation of the standard rate constant at 293 K:

$$k_{ORR}(293\text{ K}) = \begin{cases} i_0\cdot\frac{A_{eff}}{V_{ED}}\cdot\left(1-0.9\cdot\frac{q}{7}\right) & \text{for } q \le 7\ C/m^2 \\ 1.5245\ i_0\cdot\frac{A_{eff}}{V_{ED}}\cdot 10^{-0.02616q} & \text{for } q > 7\ C/m^2 \end{cases} \quad [17]$$

where i_0 is the exchange current density at 293 K,[16] and q is the quantity of discharged electricity per surface area of the electrode and is calculated from the accumulated local reaction rate and effective surface area of the electrode per volume $A_{\text{eff}}/V_{\text{ED}}$:

$$q(t) = \frac{\int R_{\text{ORR}} \cdot dt}{A_{\text{eff}}/V_{\text{ED}}} \quad [18]$$

The effective surface area of electrode per volume changes with time due to the evolution of pores and is determined by the statistics model in the following section. The function of the standard rate constant is derived based on the experimental results that the exchange current density decreases by an order of magnitude with a very small quantity of discharge (~7 C/m^2) on a glassy carbon electrode.[41] The above equation indicates that when the quantity of discharged electricity is less than 7 C/m^2, the production of Li_2O_2 sediment will gradually cover the effective surface area of the electrode and linearly decrease the standard rate constant. The continuous growth of the Li_2O_2 film further passivates the electrode and coefficients that indicate the decrease rate of the standard rate constant are also fitted from the experimental results.[41] Meanwhile, the growth of Li_2O_2 film also affects the mass transfer in the porous electrode by decreasing the pore size and porosity. The quantitative change of pore size and porosity will be discussed in the following statistics model.

Microstructural evolution of the porous electrode.— The cathode product Li_2O_2 is both insoluble and insulating, during discharge it precipitates in the porous electrode and causes electrode passivation. At the macroscopic level, the solid Li_2O_2 decreases porosity and increases transport resistance. These facts are considered in the electrolyte and oxygen concentration equations through decreased effective diffusivities and permeability. At the microscopic level, the formed Li_2O_2 film increases transport resistance of lithium ions, oxygen molecules, and electrons from the electrolyte to the electrode surface and decrease the effective surface area of the electrode (electrode passivation). In this work, the property changes due to the deposition of solid products during discharge will be studied in detail by the statistics model described below so that the effect of the electrode properties on the battery performance could be accurately determined.

The statistics model.—Porous electrodes that are widely used in energy conversion and storage devices are composed of micro-, meso-, and macro- pores with a broad range of pore sizes from less than 1 nm to more than 1 μm.[23] Therefore, changes of the electrode properties such as porosity, tortuosity, permeability, etc. will be determined as statistical characteristics of the material by a statistics model. The measured pore size in a porous electrode usually follows a log normal distribution,[21] therefore, this study applies data regression analysis and fits the measured pore distribution of a typical electrode[21] using a lognormal distribution. The probability distribution function (PDF) of pore size x in the electrode can be written as:

$$\text{PDF}(x) = \exp\left[\frac{-(\ln(x)-\mu)^2}{2\sigma^2}\right] \Big/ (\sqrt{2\pi}\cdot\sigma x) \quad \text{for } x > 0 \quad [19]$$

where the mean pore size μ and the shape factor σ are fitted from experimental data as 93 nm and 0.5.

The statistical properties such as the average pore size, d_{eff}, the surface area, A_{ED}, per volume, V_{ED}, among other parameters of the porous electrode can be calculated from the PDF of the porous electrode:

$$d_{\text{eff}} = \int_0^\infty x \cdot \text{PDF}(x) \cdot dx \quad [20]$$

$$\frac{A_{\text{eff}}}{V_{\text{ED}}} = \frac{\varepsilon \int_0^\infty \text{PDF}(x)\cdot \pi x^2 \cdot dx}{\int_0^\infty \text{PDF}(x)\cdot \frac{\pi x^3}{6}\cdot dx} \quad [21]$$

In this study, the thickness of the precipitated Li_2O_2 film is assumed identical in all pores that is larger than the critical pore size, $d_{\min}$, within the computing element. As a result, the PDF within each computing element changes to the following piece-wise function after a layer of Li_2O_2 with the thickness of $\delta_{Li_2O_2}$ deposits on the surface and decreases the diameter of a pore from x to d:

$$\text{PDF}(d) = \begin{cases} \exp\left[\frac{-(\ln(d+2\delta_{Li_2O_2}))}{2\sigma^2}\right] \Big/ \left[\sqrt{2\pi}\sigma(d+2\delta_{Li_2O_2})\right] & \text{if } x > d_{\min}+2\delta_{Li_2O_2}, d = x - 2\delta_{Li_2O_2} \\ \frac{\frac{1}{2}\text{erf}\left(\frac{\mu-\ln(d_{\min})}{\sqrt{2}\sigma}\right) - \frac{1}{2}\text{erf}\left(\frac{\mu-\ln(d_{\min}+2\delta_{Li_2O_2})}{\sqrt{2}\sigma}\right)}{2\delta_{Li_2O_2}} & \text{if } d_{\min}+2\delta_{Li_2O_2} > x > d_{\min}, d = d_{\min} \\ \exp\left[\frac{-(\ln(d)-\mu)^2}{2\sigma^2}\right] \Big/ \left(\sqrt{2\pi}\sigma d\right) & \text{if } x \le d_{\min}, d = x, \delta_{Li_2O_2} = 0 \end{cases} \quad [22]$$

Where the thickness of the Li_2O_2 film, $\delta_{Li_2O_2}$, is calculated from the cumulative ORR rate by:

$$\delta_{Li_2O_2} = \left(\frac{\int R_{\text{ORR}}\cdot dt}{2F}\cdot\frac{M_{Li_2O_2}}{\rho_{Li_2O_2}}\right) \Big/ \left(\frac{A_{\text{eff}}}{V_{\text{ED}}}\right) \quad [23]$$

All the statistical properties of the porous electrode within the computing element will be updated with the new PDF. The Li_2O_2 film has low thermal and electrical conductivities[41,42] and increases the electrical and thermal resistance between the carbon electrode and the organic electrolyte. Since the electrical conductivity of Li_2O_2 (10^{-12} to 10^{-13} S/m)[41] is much lower than that of carbon (3 S/m), the ohm resistance of the electrode is determined by the ohm resistance of Li_2O_2 film which can be calculated directly from its thickness, $\delta_{Li_2O_2}$, and the electrical conductivity of Li_2O_2.During the discharging of the battery, the thickness of the Li_2O_2 film, $\delta_{Li_2O_2}$, increases in proportion to the reaction rate, R_{ORR}, and is calculated from the difference between the effective pore size, d_{eff}, and the initial pore size. The voltage drop, or overpotential $\eta_{\text{ohm},Li_2O_2}$, caused by the ohm resistance is determined by:

$$\eta_{\text{ohm, }Li_2O_2} = \frac{\left(\delta_{Li_2O_2}/\sigma_{Li_2O_2}\right)\cdot R_{\text{ORR}}}{A_{\text{eff}}/V_{\text{ED}}} \quad [24]$$

This two-dimensional model assumes that variables along the z direction are uniform, the discharge current density, I, is calculated by integrating the ORR rates:

$$I = \frac{\int R_{\text{ORR}}\cdot dxdy}{\delta_Y} \quad [25]$$

To the author's knowledge, the change of electrode properties caused by electrochemical reactions has never been studied in detail to consider the evolution of pore size in the electrode. The statistics model in this study will quantify the effect of the precipitation of solid Li_2O_2 on the properties of the battery electrode and the resulted electrode passivation. The electrode properties determined by the statistics model will be input to the CFD model and governing equations in section Governing equations to calculate the heat and mass transfer coupled with electrochemical reactions within the electrode.

Boundary conditions.— Boundaries for the computational domain are numbered in Figure 1. The upper and lower (I) boundaries are considered to be symmetric boundaries and the corresponding boundary

conditions are:

$$\frac{\partial \Phi}{\partial y} = 0 \quad [26]$$

where Φ can be T, ω_{Li+}, and ω_{O_2}. At the lithium/separator interface (boundary II), the flux of lithium ion is proportional to the discharge current density:

$$N_{Li+} = \rho D^{eff}_{Li+} \nabla \omega_{Li+} = \frac{I}{F} M_{Li+} \quad [27]$$

The electrolyte current density i_{EL} at boundary II equals to the discharge current density I, while the electrolyte current density equals to zero at boundaries III and IV. At the electrode/rib interface (boundary III), the flux of lithium ion and oxygen are 0 and the temperature at boundary III is set as room temperature. At the electrode/channel interface (boundary IV), the concentration of lithium ion and the oxygen are set as 6.86×10^{-3} and 1.41×10^{-3} kg kg^{-1} respectively. Since the thermal resistance of lithium metal and current collectors are negligible, the temperatures at boundaries II, III, and IV are equal to the room temperature, T_∞.

The computational grids are generated based on the finite volume method (FVM)[4,3] governing equations are discretized and solved by home-made code developed with Fortran. The grid number is 165 $\times$ 20 and the time step is 1 second, all the model results are both grid independent and time step independent. After the results are converged in each time step, the cell voltage is determined by the following equation:

$$V = E_0 - \eta_C - \eta_{ohm,Li_2O_2} - I \cdot \frac{(\delta_{EL} + 0.5\delta_{ED})}{\sigma^{eff}_{ED}} \quad [28]$$

where the kinetic and concentration over-potential on cathode, η_C, is obtained through iterations at a given discharge current density I. The potential drop over the precipitated Li_2O_2 film, η_{ohm,Li_2O_2}, is calculated based on the microstructural evolution of the porous electrode, Eq. 24. It should be mentioned that the thickness of the electrode is multiplied by a factor of 0.5 in Eq. 28 to average the length of lithium ion transfer in electrode. The ohm over-potential in solid carbon phase of the cathode is neglected in current work because electron conductivity in carbon is much higher (300 S m^{-1}) than the conductivity of lithium ion in the electrolyte (0.5 S m^{-1}).

Governing equations are summarized in Table I and values of parameters used in the model are all presented in Table II. Transport properties are obtained from published data of the electrolyte of 1M $LiPF_6$ in propylene carbonate/dimethoxyethane (1:2 wt). In the following discussions, if not otherwise specified, the battery is discharged at a constant current of 1 A m^{-2}, and the ambient temperature is 293 K.

Results and Discussion

Model validation.— After the grid and time-independence verifications, the model simulates a lithium-oxygen battery with a 25-μm-thick separator and an 800-μm-thick electrode. The simulation results of discharge capacity vs. cell voltage at various discharge current densities are compared to the experiment data in Ref. 44, as shown in Figure 3. It should be noted that simulation results in Figure 3 are obtained by setting the open ratio as 100% in order to keep consistent with the experimental setup. The calculated specific capacities by our model agree well with experimental results and the following results and discussions are based on the validated model and parameters. Results of temperature distributions are not the primary concern of this study because the temperature increase is calculated to be less than 0.1 K in the current model due to the effective cooling by natural convection and low heat generation rate. The current battery model is built based on lab scale batteries with small sizes (in the order of 1 cm) and low discharge current density (in the order of 1 mA/cm^2). The temperature variation within the battery will be higher in larger batteries or battery packs.

Results in Figure 3 indicate that the cell voltage decreases with the discharge capacity due to the exacerbating electrode passivation

Table II. Parameters used in the model.

Parameter	Symbol	Value
Room temperature	T_∞	293 K
Exchange current density	i_0	3.11×10^{-6} A m^{-2}[16]
Transfer coefficient of cathode	α_{ORR}	0.5[46]
Thermodynamic equilibrium voltage	E_0	3.1[2]
Reference concentration of O_2	$\omega^{ref}_{O_2}$	1.23×10^{-4} kg kg^{-1}[16]
Reference concentration of lithium ion	ω^{ref}_{Li+}	6.86×10^{-3} kg kg^{-1}[16]
Density of PTFE	ρ_{PTFE}	2.2 g cm^{-3}
Density of lithium	ρ_{Li}	0.534 g cm^{-3}
Density of carbon	ρ_C	2.26 g cm^{-3}
Density of lithium peroxide	$\rho_{Li_2O_2}$	2.31 g cm^{-3}
Density of electrolyte	ρ_{EL}	1.011 g cm^{-3}[24]
Conductivity of electrolyte	σ_{EL}	15.9×10^{-3} S cm^{-1}[24]
Conductivity of electrode	σ_{ED}	3 S cm^{-1}[47]
Conductivity of Li_2O_2	$\sigma_{Li_2O_2}$	1×10^{-13} S cm^{-1}[48]
Specific heat of electrolyte	$Cp_{,EL}$	0.5 J g^{-1} K^{-1}
Specific heat of carbon	$Cp_{,ED}$	0.71 J g^{-1} K^{-1}
Specific heat of Li_2O_2	$Cp_{,Li_2O_2}$	1.81 J g^{-1} K^{-1}
Diffusivity of oxygen in electrolyte	D_{O_2}	8.35×10^{-6}cm^2 s^{-1}[24]
Diffusivity of Li^+ in electrolyte	D_{Li+}	8×10^{-7} cm^2 s^{-1}[47]
Thermal conductivity of electrolyte	k_{EL}	0.2 W m^{-1} K^{-1}
Thermal conductivity of electrode	k_{ED}	1.5 W m^{-1} K^{-1}
Thermal conductivity of Li_2O_2	$k_{Li_2O_2}$	14.5 W m^{-1} K^{-1}
Solubility of oxygen in electrolyte		4.45×10^{-3} M[24]
Molecular weight of lithium	M_{Li}	6.94 g mol^{-1}
Molecular weight of lithium peroxide	$M_{Li_2O_2}$	45.88 g mol^{-1}
Porosity of separator	ε_{EL}	0.5[13]
Thickness of the electrode	δ_{ED}	800 μm[44]
Thickness of the separator	δ_{EL}	25 μm[13]
Width of the battery	δ_Y	2 mm
Width of the rib	δ_{RIB}	1 mm

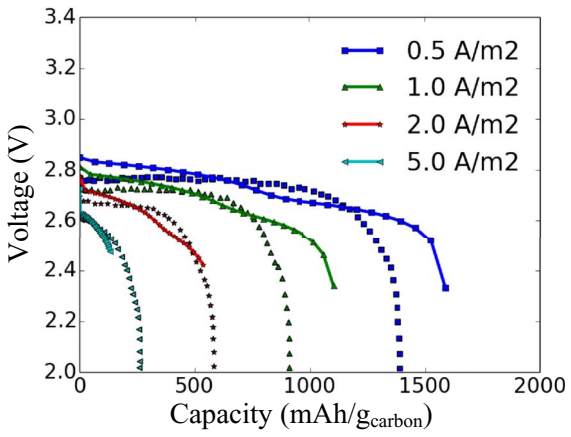

Figure 3. Discharge of a lithium-oxygen battery with an 800-μm-thick electrode at various current densities (Experimental data: scatter plots; Model simulations: lines with marker).

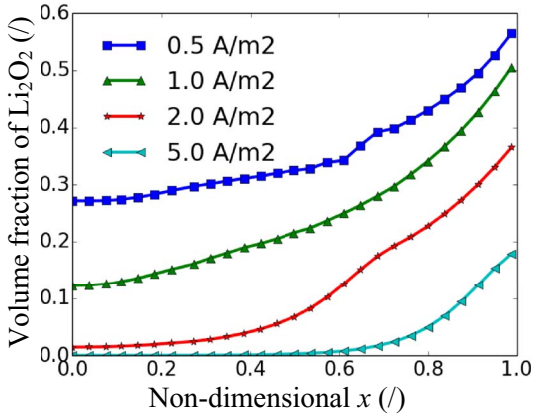

Figure 4. Volume fractions of Li_2O_2 along the thickness of the electrode at the end of the discharge. The electrode thickness is 800 μm.

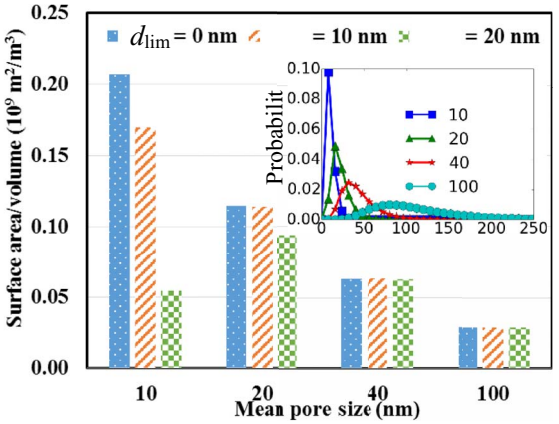

Figure 5. Effect of the pore size distributions and the critical pore size (d_{lim}) on the surface area per volume.

and increased concentration over-potential. At the first half of the discharge (the discharge capacity is less than 50% of the maximum capacity), the voltage decreases relatively fast with the capacity since the exchange current density of the electrode decreases almost linearly by 90% due to the electrode passivation by the Li_2O_2 film when the local discharge capacity is less than 7 C/cm^2. At the second half of the discharge (the discharge capacity is more than 50% of the maximum capacity), the decrease rate of the voltage was slower until the Li_2O_2 blocks the mass transfer and concentration over-potential sharply increases and dominates the voltage loss at the end of the discharge.

Figure 3 also compares battery performances under various discharge current density rates. The discharge capacity decreases from 1589.6 to 131.5 mAh/g_{carbon} when the current density increases from 0.5 to 5 A/m^2. The current density determines the consumption rate of the reactants (oxygen and lithium ion) and the oxygen flux from the channel to the gas diffusion layer is proportional to the current density. Since the electrode is flooded with liquid electrolyte, oxygen from the channel needs to dissolve in the electrolyte before it diffuses to the reaction sites in the electrode. The low solubility and diffusivity of oxygen in organic electrolytes limits the discharge current density. Furthermore, the reaction rates are not uniform in the electrode due to the concentration gradient of reactants and the non-uniformity is more significant at large discharge current rates. Therefore, the concentration over-potential increases with current densities. Figure 4 compares the volume fraction of Li_2O_2, which is proportional to the local discharge capacity, Eq. 23, along the depth of the electrode at the end of the discharge. At high discharge current densities, such as 5 A/m^2, the volume fraction of Li_2O_2 is almost 0 in the vicinity to the separator, which indicates a low utilization of the electrode. With the decrease of the discharge current, the volume fraction of Li_2O_2 increases all over the electrode, especially in the vicinity to the separator, and leads to a higher discharge capacity as shown in Figure 3.

In lithium-oxygen battery stacks, the current collectors and flow channels that transfer current and deliver oxygen would inevitably block part of the gas diffusion layer/channel interface as illustrated in Figure 1. In the following study, the open ratio of the gas diffusion layer is assumed to be 50% to simulate real-world applications and the thickness of the electrode is 800 μm. It's worth noting that, all else being equal, the discharge capacity at 50% open ratio is only one quarter of the discharge capacity at 100% open ratio due to the oxygen transfer impedance caused by the current collector.[16] In the following discussions, the simulated discharge capacity of the battery (at 50% open ratio) will be significantly lower than the experimental data reported in literature (at 100% open ratio).

Pore size distribution.— Electrodes made from commercial and home-made electrode materials have very wide pore size distributions, which are determined by the size of the raw material, amount of binding agent, and the preparation process etc. The pore size distribution measured by experiments usually follows a log normal distribution and the mean pore size varies from 10 to 120 nm.[23] In this study, electrodes with a series of pore size distributions are simulated, the mean pore size changes from 10 to 100 nm as shown in the inserted plot in Figure 5. The surface area per volume of these electrodes decreases from 0.21 to 0.03 nm^2/nm^3 when the mean pore size increases from 10 to 100 nm considering the fact that the surface area to volume ratio of smaller pores is higher than that of larger pores. On the other hand, Figure 5, the critical pore size, d_{lim}, has a more profound effect on electrodes with smaller mean pore size because a larger fraction of pores are smaller than the critical pore size. When the critical pore size increases from 0 to 20 nm, the surface area per volume decreases from 0.21 to 0.03 nm^2/nm^3 in electrodes with the mean pore size of 10 nm. While the surface area per volume keeps almost unchanged in electrodes with the mean pore size of 100 nm.

Electrodes with different pore sizes show very different discharge performance because the amount of available reaction sites and the passivation rates of the electrode are different. Figure 6 compares the discharge performance of electrodes with the mean pore size varying from 10 to 100 nm. The critical pore size, d_{min}, is assumed to be 10 nm in all cases. The change of the discharge capacity with the mean pore size is the balanced results between the mass transfer and the effective surface area: the mass transfer of oxygen and lithium ion in the electrode limits the capacity in small pores while the effective surface area and passivation of the electrode by Li_2O_2 film limits the capacity in large pores. When the mean pore size increases from 10 to to 50 nm, although the surface area per volume decreases, the discharge capacity increases from 86.6 to 214.8 mAh/g_{carbon} because large pores facilitate the oxygen and electrolyte transfer.

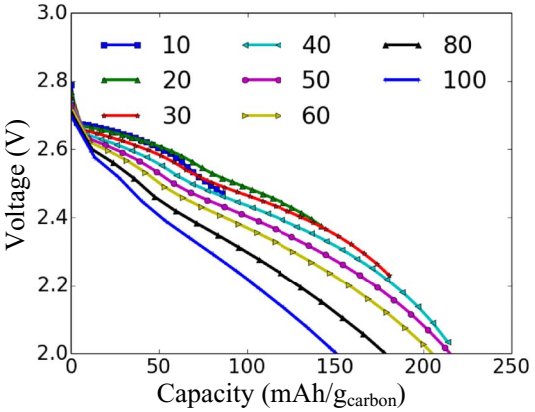

Figure 6. Discharge performance of lithium-oxygen batteries with various mean pore sizes (in nm). The critical pore size is 10 nm.

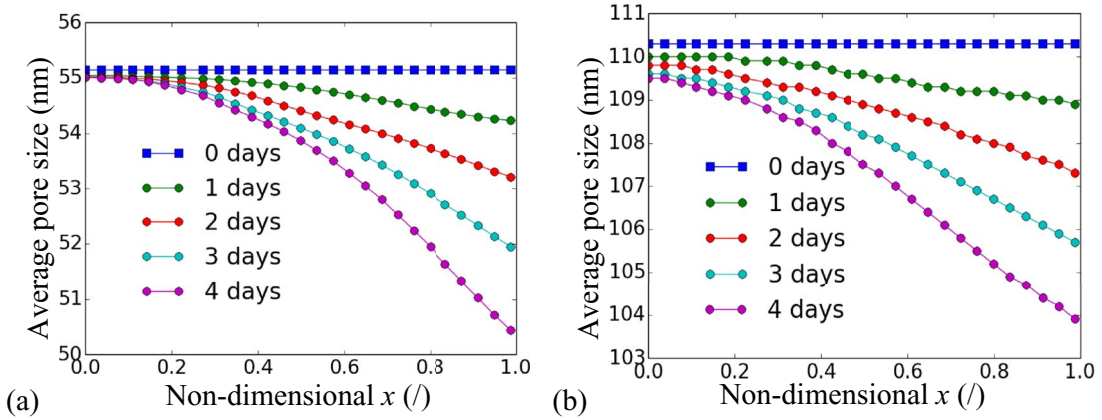

Figure 7. The change of pore size in the electrode with discharge when the mean pore size is (a) 50 nm and (b) 100 nm respectively. The thickness of the electrode is 800 μm and the critical pore size is 10 nm.

When the mean pore size is further increased to 100 nm, the discharge capacity decreased to 150.8 mAh/g_{carbon} due to the decrease of effective surface area. A smaller effective surface area leads to a high activation over-potential and a faster deposition of Li_2O_2 film on the electrode surface, and eventually decreases the discharge voltage and capacity. Figure 7 shows mean pore sizes along the depth of the electrode at various states of discharge in electrodes with the mean pore size of 50 nm (a) and 100 nm (b). Pore sizes decrease over the state of discharge due to the precipitation of Li_2O_2 film. Moreover, pore sizes decrease faster in the vicinity of oxygen channel because the reaction rate is higher. It can also be seen that the deposited Li_2O_2 film is always thinner in electrodes with a smaller mean pore size (50 nm) than that in the electrode with a larger mean pore size (100 nm) at the same state of discharge. The thinner Li_2O_2 film in Figure 7a results from the higher surface area per volume (0.05 vs. 0.03 nm^2/nm^3 considering the critical pore size and the porosity). At the end of the discharge, the average thickness of Li_2O_2 film along the depth of electrode only grows to less than 2.4 nm in the electrode with 50 nm mean pore size, while the average Li_2O_2 film thickness is up to 3.2 nm in the electrode with 100 nm mean pore size. A thicker Li_2O_2 film leads to a more severe electrode passivation and faster voltage decrease. Therefore, the discharge capacity of the electrodes decreases with the increase of pore size when the mean pore size is more than 50 nm. Meanwhile, the effective surface area of the electrode also changes with the depth of discharge due to the change of the pore size distribution. Figure 8 shows the distributions of A_{eff}/V_{ED} at the end of the discharge when the mean pore size is 50 nm and 100 nm respectively. The effective surface area per volume of electrode changes faster in electrodes with smaller mean pore size since the relative change of the pore size is higher. At the end of the discharge, Figure 8, the effective surface area per volume varies from 0.036 to 0.052 nm^2/nm^3 in the 50-nm electrode, while the value only varies from 0.025 to 0.029 nm^2/nm^3 in the 100-nm electrode.

The overall discharge capacity balances between the high surface area (which is inversely proportional to the pore size) and high reactant diffusivity (which is proportional to the pore size). The change of discharge capacity with the pore size is consistent with experimental data published in literature that when the pore size is small (2.3 to 5.5 nm) the discharge capacity increases with the increasing pore size,[26] while the discharge capacity maximizes at a medium pore size (80 nm) when the pore size varies from 2.4 to 120 nm.[27] This study also compares the activation and ohm over-potentials in electrodes with various pore sizes at the end of the discharge in Figure 9. The ohm over-potential gradually increases with the increase of the mean pore size because 1) the Li_2O_2 film is thicker in electrodes with smaller effective surface areas at the same quantity of discharge (C/m^2) and 2) the local current density (A/m^3) is larger in electrode with smaller effective surface areas at the same current density (A/m^2). The combined results lead to higher ohm over-potentials in electrodes with larger pore sizes. Meanwhile, the activation over-potential is almost linearly proportional to the discharge capacity. The electrode passivation caused by the Li_2O_2 film gradually decreases the standard rate constant, k_{ORR}, therefore, the activation loss increases with the increase of the discharge capacity. The ratio of the ohm over-potential

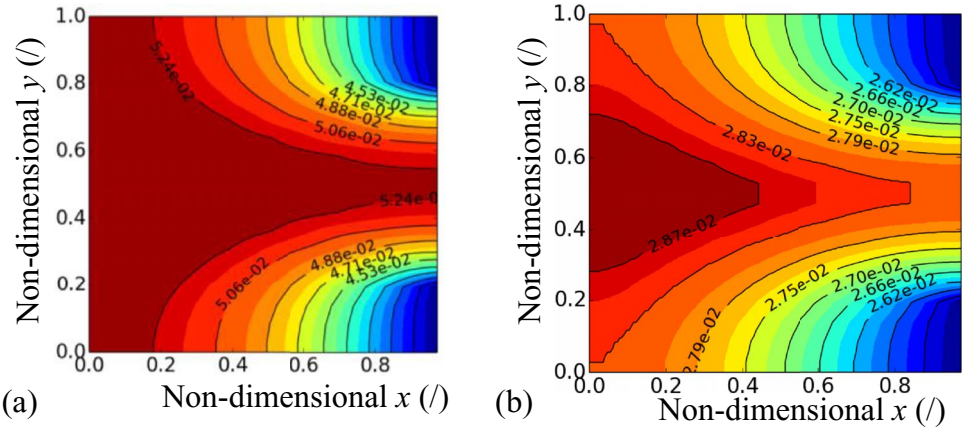

Figure 8. The distribution of effective area per volume of electrode, A_{eff}/V_{ED} (nm^2/nm^3), in the electrode at the end of discharge when the mean pore size is (a) 50 nm and (b) 100 nm respectively. The thickness of the electrode is 800 μm and the critical pore size is 10 nm.

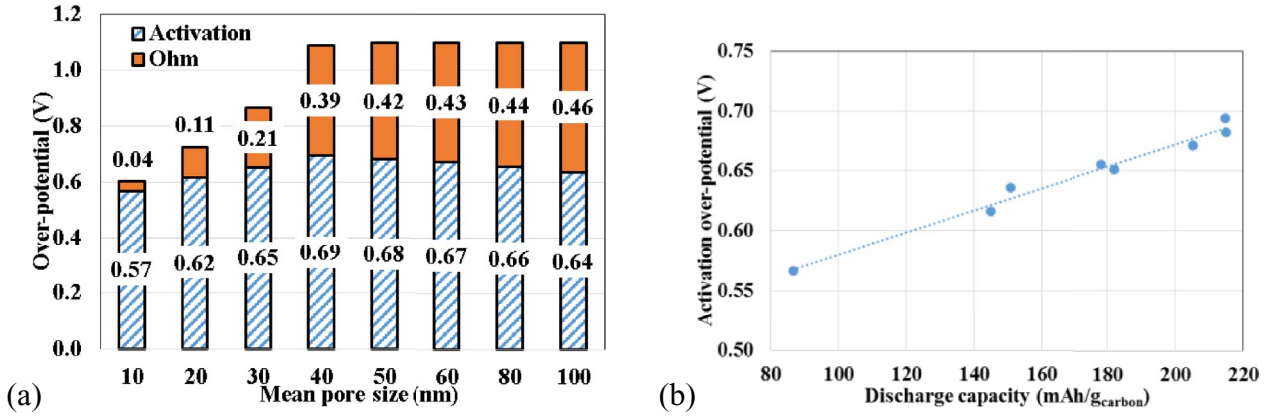

Figure 9. (a) Activation and ohm over-potential of electrodes with various mean pore size and (b) activation over-potential vs. discharge capacities at the end of the discharge. The electrode thickness is 800 μm and the discharge current is 1 A/m^2.

to activation over-potential continuously increases from 6% to 42% when the pore size increases from 10 to 100 nm, which indicates that electrodes with larger pore sizes are more sensitive to the conductivity of the Li_2O_2 film. The effect of conductivity of the Li_2O_2 film will be discussed in detail in section Resistance of the Li_2O_2.

Critical pore size.— In reality, not all pores are useful during the discharge and charge of the battery due to the limited mass transfer within small pores. It is hypothesized that pores smaller than the critical pore size, d_{lim}, do not hold electrochemical reactions and do not contribute to the battery capacity. To investigate the effect of critical pore size, this study varies the critical pore size between 0 and 30 nm (since the critical pore size could be as large as 30 nm).[20] By increasing the critical pore size, the effective surface area per volume of the electrode decreases as shown in Figure 5, which results to a faster growth of the Li_2O_2 film. The severe passivation of the electrode by Li_2O_2 film decreases the discharge capacity at a given current rate, as shown in Figure 10. When the mean pore size is 10 nm, the discharge capacity of the battery sharply decreases from 89.8 to 5.9 mAh/g_{carbon} when the critical pore size increases from 0 to 30 nm.

On the other hand, the impact of the critical pore size is very small in electrodes with large pore sizes since only a small fraction of pores are smaller than the critical pore size. When the critical pore size is set as 30 nm, 99.3% of pores are smaller than the critical pore size in electrodes with a mean pore size of 10 nm, while only 0.4% of the pores is smaller than the critical pore size in electrodes with a mean pore size of 100 nm. As a result, the discharge capacity only slightly decreases from 151.1 to 147.6 mAh/g_{carbon} in the electrode with 100 nm mean pore size when the critical pore size increases from 0 to 30 nm.

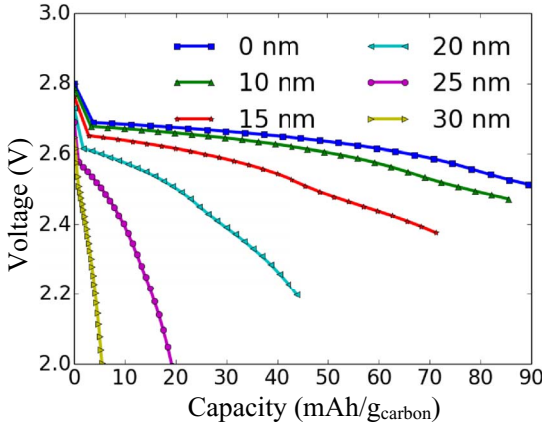

Figure 10. Discharge performance of an 800-μm-thick electrode with a mean pore size of 10 nm at the current density of 1 A/m^2, while the critical pore size varies from 0 to 30 nm.

Resistance of the Li_2O_2.— The electrode passivation is caused by the precipitation of Li_2O_2 film on the surface of the electrode and the electric conductivity of this film is critical to determine the activation and ohm over-potential. The model study conducted by Radin and Siegel[45] indicates that the conductivity of Li_2O_2 film varies during discharge and charge because the cell potential impacts defect concentrations. This model investigates the sensitivity of the electrical conductivity of the Li_2O_2 film on the discharge capacity by changing its electrical conductivity from 10^{-13} to 10^{-12} S/m. In electrodes with a mean pore size of 10 nm, the deposited Li_2O_2 film is very thin (less than 2 nm). Therefore, the change of electric conductivity of the Li_2O_2 film does not significantly change the discharge capacity or voltage of the battery, Figure 11a. In electrodes with a mean pore size of 100 nm, however, the Li_2O_2 film could grow up to 12 nm. Therefore, the discharge voltage increases with the electrical conductivity of the Li_2O_2 film, Figure 11b. The discharge capacity also increases from 150.9 to 337.8 mA/g_{Carbon} with the increase of the electric conductivity of Li_2O_2 film from 10^{-13} to 10^{-12} S/m when the cut off voltage is 2.0 V.

Alternating discharge current.— As mentioned before, the mass transfer of oxygen within the electrode limits the discharge capacity, especially at high discharge current rates. With the initial oxygen concentration of 1.23×10^{-4} kg/kg, or 3.886 mol/m^3, it is calculated using values of parameter in Table II that the oxygen will be depleted within about 10 min at the current density of 1 A/m^2 if there is no oxygen transfers from the channel:

$$\text{Time [second]} = \frac{\omega_{O_2}^{ref}}{i/(2F \cdot \delta_{ED})} \quad [29]$$

At the current rate of 1 A/m^2, the calculated maximum oxygen diffusion rate, 4.56×10^{-6} mol/(m^2 . s), from the channel to the electrode is less than the oxygen consumption rate, 5.18×10^{-6} mol/(m$^2 \cdot$ s). As a result, the oxygen concentration gradually decreases with time from 1.23×10^{-4} to less than 1.0×10^{-15} kg/kg (the gray line with square markers in Figure 12) and the discharging voltage decreases during the discharge. This study proposes an approach to increase the oxygen concentration within the electrode and increase the discharge capacity by discharging the battery under current rates alternating between 0 and the setting current.

Figure 12 compares the oxygen concentration in the vicinity of the separator when the battery discharges at a constant current rate of 1 A/m^2 and alternating current rates between 0 and 1 A/m^2 every

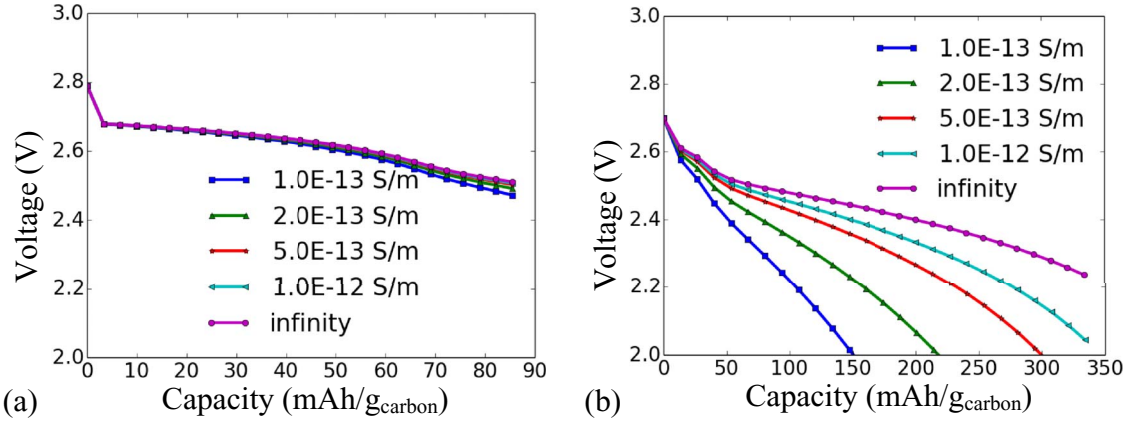

Figure 11. Discharge performance of an 800-μm-thick electrode with a mean pore size of (a) 10 nm and (b) 100 nm at the current density of 1 A/m^2, the critical pore size is assume to be 10 nm. The electric conductivity of the Li_2O_2 film varies from 10^{-12} to 10^{-13} S/m.

6 min. When the discharge current is 0, the battery is at the open circuit condition, no oxygen is consumed in the electrode while the oxygen can still diffuse from the channel into the electrode driven by the concentration gradient. Therefore, the oxygen concentration increases (the orange curve and the embedded plot in Figure 12) at the open circuit condition. The maximum oxygen concentration in Figure 12a only decreases from 1.23×10^{-4} to 6.48×10^{-6} kg/kg in the electrode with a mean pore size of 10 nm at alternating current rates. The periodic increase of oxygen concentration, when the battery is at rest, leads to a better utilization of the electrode. As a result, the discharge capacity increases from 93.15 to 225.8 mAh/g$_{carbon}$ in Figure 12a when the alternating discharge current rates are applied to an electrode with a mean pore size of 10 nm. Since the effective diffusivity of oxygen is closely related to the porosity of the electrode, in electrodes with a larger mean pore size (100 nm), the oxygen concentration increases faster when the battery is at rest so that more oxygen is available for the reaction at 1 A/m^2. The oxygen concentration in an electrode with a mean pore size of 100 nm (Figure 12b) only decreases from 1.23×10^{-4} to 1.92×10^{-5} kg/kg in the 100-nm electrode at the end of the discharge. The discharge capacity increases from 151.0 to 278.9 mAh/g$_{carbon}$ when discharge current rates alternate between 0 and 1 A/cm^2, compared with a constant discharge current of 1 A/m^2. It can also be seen from Figure 12 that the oxygen concentration is much higher in the electrode with alternating discharge current rates than that with a constant discharge current. Figure 12 only compares electrodes with the mean pore sizes of 10 nm and 100 nm. The effect of alternating discharge current rates on the performance of electrodes with mean pore sizes between 10 nm and 100 nm falls in between these two cases.

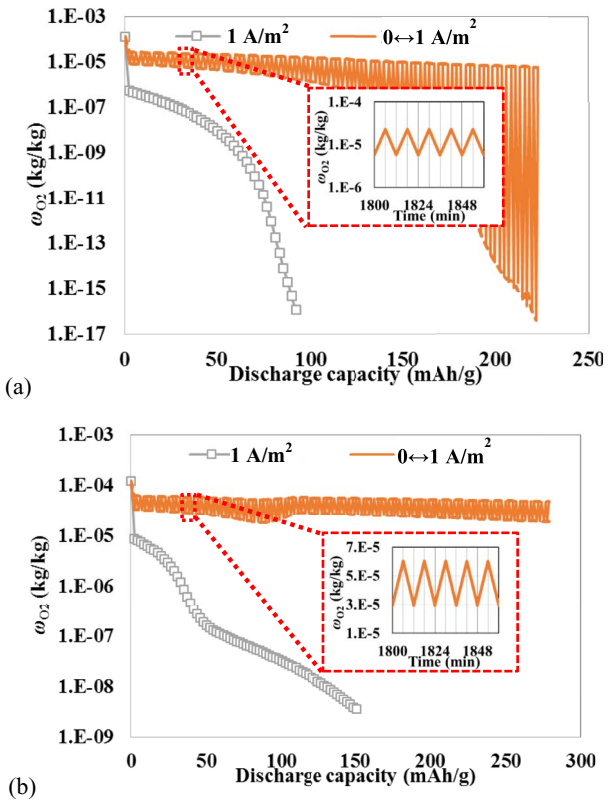

Figure 12. Oxygen concentration in the electrode in the vicinity of the separator of an 800-μm-thick electrode with a mean pore size of (a) 10 nm and (b) 100 nm at a constant current density of 1 A/m^2 (the gray line with markers) and when the current density alternates between 0 and 1 A/m^2 every 6 min (the orange curve).

In practical applications, thousands of batteries will connect in series and/or parallel to make battery modules. Batteries can be grouped and controlled independently during discharge so that a fraction of batteries discharge at high current rates while the remaining of batteries rest under the open circuit condition to absorb oxygen from the channel. Batteries under discharge and batteries at rest switch every few minutes so that the whole battery module has constant discharge current, voltage, and power. As shown in Figure 12, the specific discharge capacity of each single battery doubles using this alternating discharge method. Therefore fewer numbers of batteries are needed to achieve the same discharge capacity, which decreases both the size and weight of the battery module.

Conclusions

The pore size distribution in lithium-air battery electrodes changes because the solid product, Li_2O_2, precipitates on the electrode surface. This study develops a statistics model to consider the pore size evolution in lithium-oxygen battery electrodes with 800 μm thickness discharged at 1 A/m^2. The statistics model is also coupled with a CFD model to simulate the heat and mass transfer within the electrode and calculate the discharge performance of the battery. In addition, this study considers the fact that electrodes have various pore size distributions and micro-, meso-, and macro- pores play different roles on the mass transfer and reactions in the electrode. The model can accurately simulate battery performance and can differentiate electrodes with same macroscopic properties, such as porosity, but different microscopic properties such as pore size distributions. After being validated with experimental data published in literature, the model developed

in this study has been run at various scenarios to make the following conclusions:

1) The optimized pore size of the electrode should balance the effective surface area and the diffusive resistance of reactants (oxygen and lithium ion). The combined effects of the mass transfer limitation and electrode passivation leads to an increase of discharge capacity from 86.6 to 214.8 mAh/g_{carbon} when the mean pore size increases from 10 to 50 nm and a decrease of discharge capacity to 150.8 mAh/g_{carbon} when the mean pore size further increases to 100 nm.
2) Increasing the critical pore size from 0 to 30 nm will significantly decrease the discharge capacity of battery from 89.8 to 5.9 mAh/g_{carbon} when the mean pore size of the electrode is small (10 nm). While the critical pore size has negligible impacts on the discharge capacity of battery if the mean pore size of the electrode is relatively large (100 nm).
3) The electrode passivation caused by the Li_2O_2 film precipitates on the electrode is more sever in electrodes with large pores because the Li_2O_2 film grows thicker during discharge. The thickness of the Li_2O_2 film could grow up to 12 nm in electrodes with a mean pore size of 100 nm, while the Li_2O_2 film thickness is less than 2 nm in electrodes with a mean pore size of 10 nm.
4) Electrodes with the same porosity but different pore size distribution show different performance due to the electrode passivation. The low surface area of electrodes with larger pore sizes leads to a more severe electrode passivation. In these electrodes, the electric conductivity of the Li_2O_2 film has a significant impact on its discharge capacity.
5) The discharge capacity of the battery increases when the battery periodically rests at the open circuit condition to facilitate oxygen transfer into the electrode from the channel. When the battery discharges at 1 A/m^2, the capacity doubles if the battery periodically rests at open circuit condition every 6 min.

References

1. G. Girishkumar, B. McCloskey, A. C. Luntz, S. Swanson, and W. Wilcke, Lithium-Air Battery: Promise and Challenges. *J. Phys. Chem. Lett.* **1**, 2193 (2010).
2. K. M. Abraham, A Polymer Electrolyte-Based Rechargeable Lithium/Oxygen Battery. *J. Electrochem. Soc.* **143**, 1 (1996).
3. S. A. Freunberger, et al., The Lithium–Oxygen Battery with Ether-Based Electrolytes. *Angew. Chem. Int. Ed.* **50**, 8609 (2011).
4. B. D. McCloskey, D. S. Bethune, R. M. Shelby, G. Girishkumar, and A. C. Luntz, Solvents' Critical Role in Nonaqueous Lithium–Oxygen Battery Electrochemistry. *J. Phys. Chem. Lett.* **2**, 1161 (2011).
5. S. A. Freunberger, et al., Reactions in the Rechargeable Lithium-O_2 Battery with Alkyl Carbonate Electrolytes. *J. Am. Chem. Soc.* **133**, 8040 (2011).
6. Y. Shao, et al., Electrocatalysts for Nonaqueous Lithium−Air Batteries: Status, Challenges, and Perspective. *ACS Catal.* **2**, 844 (2012).
7. J. P. Zheng, R. Y. Liang, M. Hendrickson, and E. J. Plichta, Theoretical energy density of Li-air batteries. *J. Electrochem. Soc.* **155**, A432 (2008).
8. J. Read, et al., Oxygen Transport Properties of Organic Electrolytes and Performance of Lithium/Oxygen Battery. *J. Electrochem. Soc.* **150**, A1351 (2003).
9. X. Ren, S. S. Zhang, D. T. Tran, and J. Read, Oxygen reduction reaction catalyst on lithium/air battery discharge performance. *J. Mater. Chem.* **21**, 10118 (2011).
10. A. Debart, J. Bao, G. Armstrong, and P. G. Bruce, An O_2 cathode for rechargeable lithium batteries: The effect of a catalyst. *J. Power Sources* **174**, 1177 (2007).
11. S. S. Zhang, D. Foster, and J. Read, Discharge characteristic of a non-aqueous electrolyte Li/O_2 battery. *J. Power Sources* **195**, 1235 (2010).
12. Y.-C. Lu, H. A. Gasteiger, M. C. Parent, V. Chiloyan, and Y. Shao-Horn, The Influence of Catalysts on Discharge and Charge Voltages of Rechargeable Li–Oxygen Batteries. *Electrochem. Solid-State Lett.* **13**, A69 (2010).
13. X. Ren, S. S. Zhang, D. T. Tran, and J. Read, Oxygen reduction reaction catalyst on lithium/air battery discharge performance. *Journal of Materials Chemistry* **21**, 10118 (2011).
14. K. Huang, Y. Li, and Y. Xing, Increasing round trip efficiency of hybrid Li–air battery with bifunctional catalysts. *Electrochimica Acta* **103**, 44 (2013).
15. D. Aurbach, *Nonaqueous Electrochemistry*. (CRC Press, 1999).
16. X. Li and A. Faghri, Optimization of the Cathode Structure of Lithium-Air Batteries Based on a Two-Dimensional, Transient, Non-Isothermal Model. *J. Electrochem. Soc.* **159**, A1747 (2012).
17. Y. Wang, Modeling Discharge Deposit Formation and Its Effect on Lithium-air Battery Performance. *Electrochimica Acta* **75**, 239 (2012).
18. A. A. Franco and K.-H. Xue, Carbon-Based Electrodes for Lithium Air Batteries: Scientific and Technological Challenges from a Modeling Perspective. *ECS J. Solid State Sci. Technol.* **2**, M3084 (2013).
19. V. Y. Nimon, S. J. Visco, L. C. D. Jonghe, Y. M. Volfkovich, and D. A. Bograchev, Modeling and Experimental Study of Porous Carbon Cathodes in Li-O_2 Cells with Non-Aqueous Electrolyte. *ECS Electrochem. Lett.* **2**, A33 (2013).
20. S. R. Younesi, S. Urbonaite, F. Björefors, and K. Edström, Influence of the cathode porosity on the discharge performance of the lithium–oxygen battery. *J. Power Sources* **196**, 9835 (2011).
21. Z. Yu, R. N. Carter, and J. Zhang, Measurements of Pore Size Distribution, Porosity, Effective Oxygen Diffusivity, and Tortuosity of PEM Fuel Cell Electrodes. *Fuel Cells* **12**, 557 (2012).
22. P. Tan, W. Shyy, L. An, Z. H. Wei, and T. S. Zhao, A gradient porous cathode for non-aqueous lithium-air batteries leading to a high capacity. *Electrochem. Commun.* **49**, 111 (2014).
23. M. Olivares-Marín, P. Palomino, E. Enciso, and D. Tonti, Simple Method to Relate Experimental Pore Size Distribution and Discharge Capacity in Cathodes for Li/O_2 Batteries. *J. Phys. Chem. C* **21**, 20772 (2014).
24. J. Read, et al., Oxygen Transport Properties of Organic Electrolytes and Performance of Lithium/Oxygen Battery. *J. Electrochem. Soc.* **150**, A1351 (2003).
25. J. Christensen, et al., A Critical Review of Li/Air Batteries. *J. Electrochem. Soc.* **159**, R1 (2011).
26. C. Tran, X.-Q. Yang, and D. Qu, Investigation of the gas-diffusion-electrode used as lithium/air cathode in non-aqueous electrolyte and the importance of carbon material porosity. *J. Power Sources* **195**, 2057 (2010).
27. N. Ding, et al., Influence of carbon pore size on the discharge capacity of Li–O_2 batteries. *J. Mater. Chem. A* **2**, 12433 (2014).
28. J. Yuan, J. Yu, and B. Sunden, Review on mechanisms and continuum models of multiphase transport phenomena in porous structures of non-aqueous Li-Air batteries. *J. Power Sources* **278**, 352 (2015).
29. S. S. Sandhu, J. P. Fellner, and G. W. Brutchen, Diffusion-limited model for a lithium/air battery with an organic electrolyte. *J. Power Sources* **164**, 365 (2007).
30. P. Albertus, et al., Identifying Capacity Limitations in the Li/Oxygen Battery Using Experiments and Modeling. *J. Electrochem. Soc.* **158**, A343 (2011).
31. P. Andrei, J. P. Zheng, M. Hendrickson, and E. J. Plichta, Some Possible Approaches for Improving the Energy Density of Li-Air Batteries. *J. Electrochem. Soc.* **157**, A1287 (2010).
32. U. Sahapatsombut, H. Cheng, and K. Scott, Modelling the micro–macro homogeneous cycling behaviour of a lithium–air battery. *J. Power Sources* **227**, 243 (2013).
33. K.-H. Xue, T.-K. Nguyen, and A. A. Franco, Impact of the Cathode Microstructure on the Discharge Performance of Lithium Air Batteries: A Multiscale Model. *J. Electrochem. Soc.* **161**, E3028 (2014).
34. K.-H. Xue, E. McTurk, L. Johnson, P. G. Bruce, and A. A. Franco, A Comprehensive Model for Non-Aqueous Lithium Air Batteries Involving Different Reaction Mechanisms. *J. Electrochem. Soc.* **162**, A614 (2015).
35. X. Li, J. Huang, and A. Faghri, Modeling study of a Li–O_2 battery with an active cathode. *Energy* **81**, 489 (2015).
36. Y. Wang and S. C. Cho, Analysis and Multi-Dimensional Modeling of Lithium-Air Batteries. *J. Electrochem. Soc.* **162**, A114 (2015).
37. R. R. Mitchell, B. M. Gallant, C. V. Thompson, and Y. Shao-Horn, All-carbon-nanofiber electrodes for high-energy rechargeable Li–O_2 batteries. *Energy Environ. Sci.* **4**, 2952 (2011).
38. X. Li and A. Faghri, Local entropy generation analysis on passive high-concentration DMFCs (direct methanol fuel cell) with different cell structures. *Energy* **36**, 403 (2011).
39. M. Matyka, A. Khalili, and Z. Koza, Tortuosity-porosity relation in porous media flow. *Phys. Rev. E - Stat. Nonlinear Soft Matter Phys.* **78**, (2008).
40. A. B. Anderson, et al., Activation energies for oxygen reduction on platinum alloys: Theory and experiment. *J. Phys. Chem. B* **109**, 1198 (2005).
41. V. Viswanathan, et al., Electrical conductivity in Li_2O_2 and its role in determining capacity limitations in non-aqueous Li-O_2 batteries. *J. Chem. Phys.* **135**, 214704 (2011).
42. Y.-C. Lu and Y. Shao-Horn, Probing the Reaction Kinetics of the Charge Reactions of Nonaqueous Li–O_2 Batteries. *J. Phys. Chem. Lett.* **4**, 93 (2013).
43. S. Patankar, *Numerical Heat Transfer and Fluid Flow*. (CRC Press, 1980).
44. J. Read, Characterization of the lithium/oxygen organic electrolyte battery. *J. Electrochem. Soc.* **149**, A1190 (2002).
45. R. Maxwell and S. Donald, Charge transport in lithium peroxide: relevance for rechargeable metal–air batteries. *Energy Environ. Sci.* **6**, 2370 (2013).
46. C. M. O'Laoire, Investigations of oxygen reduction reactions in non-aqueous electrolytes and the lithium-air battery. 172 (Northeastern University, 2010).
47. Y.-C. Lu, et al., The discharge rate capability of rechargeable Li-O_2 batteries. *Energy & Environmental Science* **4**, 2999 (2011).
48. Y.-C. Lu and Y. Shao-Horn, Probing the Reaction Kinetics of the Charge Reactions of Nonaqueous Li-O_2 Batteries. *J. Phys. Chem. Lett.* **4**, 93 (2013).